Observation of a variable sub-THz radiation driven by a low energy electron beam from a thermionic rf electron gun

A. V. Smirnov,[1,*] R. Agustsson,[1] W. J. Berg,[2] S. Boucher,[1] J. Dooling,[2] T. Campese,[1] Y. Chen,[1] L. Erwin,[2] B. Jacobson,[1] J. Hartzell,[1] R. Lindberg,[2] A. Murokh,[1] F. H. O'Shea,[1] E. Spranza,[1] S. Pasky,[2] M. Ruelas,[1] N. S. Sereno,[2] Y. Sun,[2] and A. A. Zholents[2]

[1]*RadiaBeam Technologies LLC, 1717 Stewart Street, Santa Monica, California 90404, USA*
[2]*Advanced Photon Source, Argonne National Laboratory, Argonne, Illinois 60439, USA*
(Received 13 May 2015; published 29 September 2015)

We report observations of an intense sub-THz radiation extracted from a ~3 MeV electron beam with a flat transverse profile propagating between two parallel oversized copper gratings with side openings. Low-loss radiation outcoupling is accomplished using a horn antenna and a miniature permanent magnet separating sub-THz and electron beams. A tabletop experiment utilizes a radio frequency thermionic electron gun delivering a thousand momentum-chirped microbunches per macropulse and an alpha-magnet with a movable beam scraper producing sub-mm microbunches. The radiated energy of tens of micro-Joules per radio frequency macropulse is demonstrated. The frequency of the radiation peak was generated and tuned across two frequency ranges: (476–584) GHz with 7% instantaneous spectrum bandwidth, and (311–334) GHz with 38% instantaneous bandwidth. This prototype setup features a robust compact source of variable frequency, narrow bandwidth sub-THz pulses.

DOI: 10.1103/PhysRevSTAB.18.090703 PACS numbers: 41.60.Ap, 41.20.Gz, 41.60.Cr

I. INTRODUCTION

The terahertz (THz) range of the electromagnetic spectrum is energetically equivalent to photon energies of several millielectronvolts, hence the relevance of THz waves for selective excitation of low energy collective modes in correlated materials and control of materials through field manipulation of electronic, atomic, and spin degrees of freedom. Other applications of the THz waves include chemical sensing and identification, biological and medical imaging, and homeland security, where the THz wave is mainly used as a probe [1]. High power THz radiation is usually produced by means of a coherent undulator radiation in free electron lasers [2], transition radiation in linacs [3–6], or synchrotron radiation in electron storage rings [7,8]. But, these facilities are large, expensive, and not readily available on a customized base for a broader community of researchers and industrial users. There exist compact sub-mm wave sources [9], i.e., the laser driven photoconductive antennas, molecular and solid state lasers, gyrotrons, miniature tubes such as backward wave oscillators (BWO) and extended interaction klystrons (EIK). However, typical drawbacks of these sources are a low peak power and/or a low repetition rate. Therefore, there is a strong demand for compact tabletop sources in the THz frequency range with substantial average and peak power.

Coherent Cherenkov radiation (CCR) can be an attractive alternative to the coherent undulator radiation for the generation of narrow bandwidth THz waves. In the University of California, Los Angeles (UCLA) experiment [10], a 11 MeV electron beam from a laser-driven radio frequency (rf) photoinjector produced up to 10 μJ per rf macropulse at about mm wavelength radiation using a magnetic chicane for electron bunch compression and a 1-cm long quartz capillary tube. Radiation with a central frequency of 273 or 376 GHz and bandwidth of 7%–10% was produced using one or another metallized capillary tube with corresponding wall thickness. Note that once the capillary tube is installed the radiation frequency is not tunable as the beam is essentially relativistic, whereas the group velocity is relatively low.

In such a CCR sub-THz source, the radiation coherence is provided by the following three conditions satisfied simultaneously: (a) existence of an eigenmode with substantial interaction efficacy supported along the bounded interaction region of hundreds of wavelengths; (b) Cherenkov synchronism between the charged particle beam and the eigenmode supported along the region; and (c) presence of substantial sub-THz components in the beam current spectrum (e.g., a sub-ps electron bunch). Obviously, these conditions can be realized in various ways and more than a single wavelength can, in principle, be radiated from the same structure.

The experiment described here implements these conditions in a somewhat diverse way. A thermionic electron rf gun generates a long train of momentum-chirped electron

*asmirnov@radiabeam.com

Published by the American Physical Society under the terms of the Creative Commons Attribution 3.0 License. Further distribution of this work must maintain attribution to the author(s) and the published article's title, journal citation, and DOI.

bunches which are compressed in an alpha-magnet. A coherent Vavilov-Cherenkov radiation is produced downstream of the alpha-magnet in a planar, partially open slow-wave structure. It comprises a pair of electrically wide, horizontally unbounded, about a wavelength vertical gap, dielectric-free, high aspect ratio, metal gratings. Thus neither self-microbunching, such as free electron laser (FEL) process, nor BWO self-oscillation is used.

The modes capable of interacting with the beam are limited by discrete eigenmodes whose frequencies are defined by a close proximity of the phase velocity to the beam velocity and also by a quasioptical rarefaction of the eigenmode spectrum (being quasicontinuous for open structures).

The mechanism of the electron beam interaction with the radiation also differs from diffraction radiation devices operating in a semiopen configuration with electrically large gaps sufficient for propagation and interference of spherical waves. Among these devices are Smith-Purcell, orotrons, klinotrons, etc. Thus the gratings employed here act solely as a slow wave structure (i.e., not as a diffraction or Bragg system).

To the best of our knowledge, an intense, tunable coherent radiation with a sub-mm wavelength has not yet been produced using a completely laser-free and undulator-free tabletop system with a few MeV electron beam. This paper presents direct observation of sub-THz-range coherent Cherenkov radiation produced in a robust, tabletop system highlighting a novel flexible utility for compact thermionic injectors.

II. EXPERIMENTAL SETUP

The experiment was jointly developed by RadiaBeam Technologies, LLC and the Accelerator Systems Division of Advanced Photon Source (APS) at Argonne National Laboratory (ANL) and conducted in the Injector Test Stand (ITS) of the APS. Figure 1 shows a schematic of the experimental setup. The electron bunches are accelerated to an energy of approximately 3 MeV and momentum chirped in the 1.5-cell, 2.856 GHz rf thermionic electron gun. This chirp is used for a longitudinal compression of the electron bunches by an alpha-magnet. To generate short electron bunches, low energy electrons are scraped off inside the alpha-magnet vacuum chamber.

A set of quadrupole lenses is used to control vertical and horizontal beam envelops in the beam line, as shown in Fig. 2(a), and for obtaining a quasiflat beam transverse profile in the sub-THz radiator shown in Fig. 2(b). The Cherenkov radiation outcoupled from the radiator system is transported to the interferometer by means of three off-axis parabolic mirrors.

The alpha-magnet has a minimum magnetic gap of 2.2 cm and a maximum gradient of the magnetic field of 4 T/m at an excitation current of 16.4 A, limited by an air cooling. The magnet height, width and length are 35, 25 and 28 cm, respectively. The measured magnetic field errors are less than 0.63% rms. The alpha-magnet vacuum chamber includes a scraper to collimate the low energy portion of the beam. An actuator driven scraper position is remotely controlled in the range of (8.3–17.3) cm with

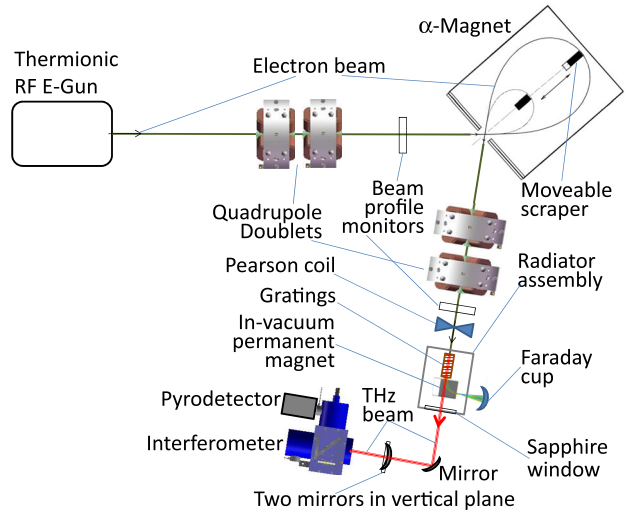

FIG. 1. Schematic layout of the experimental setup. Five beam steering correctors are not shown. The layout footprint is about (1×1.5) m^2.

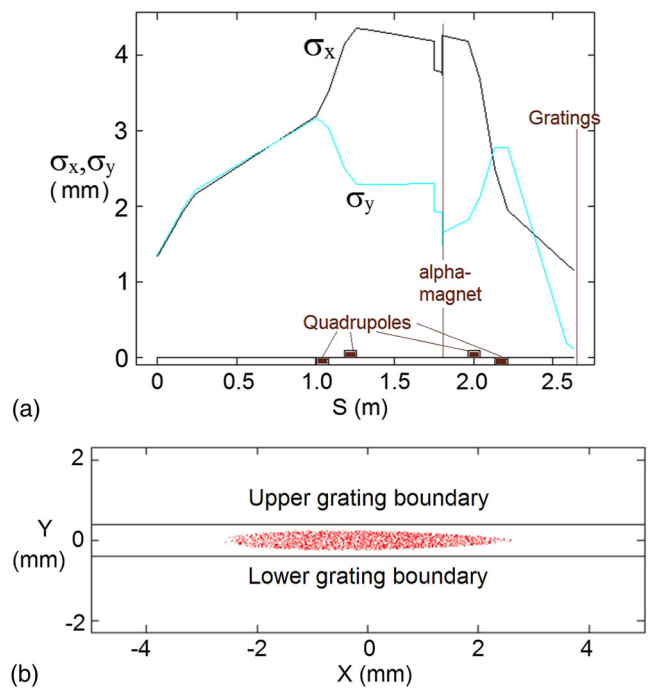

FIG. 2. Beam rms envelopes (a) and the beam transverse profile (b) simulated with ELEGANT [11] for a case of the "flat" beam lattice. Quadrupole gradients are (from left to right) −0.31, 0.28, 0.39, −0.63 T/m. The alpha-magnet with 2.53 T/m gradient is placed at $S \approx 1.8$ m and denoted with a vertical line. Beam scraping is 60%. The averaged beam kinetic energy from the rf gun is 2.6 MeV.

TABLE I. Beam parameters of the RBT-ANL experimental setup at APS/ITS.

Averaged beam kinetic energy	E	2.5–3 MeV
E-gun macropulse beam current	I	up to 400 mA
rf pulse repetition rate	ν	6–15 Hz
Beam macropulse duration FWHM	t_p	~250 ns
Bunch charge on the Faraday cup	q	up to 30 pC
Minimum rms bunch duration	σ_t	<1 ps

respect to the entrance of the alpha-magnet. The alpha-magnet vacuum chamber is supplied with two beam ports of 2.18 cm aperture and enables trajectory depths up to 16 cm, with the vertical aperture ranging from 1.79 to 2.18 cm.

The experiment was conducted with the electron beam and beam line parameters given in Table I. Prior to obtaining the sub-THz radiation, the electron beam was aligned using five steering coils and centered within the 0.8 mm gap between gratings of the sub-THz radiator. The quadrupole gradients were preset using the values defined from beam transport simulations [see Fig. 2(a)]. The transverse shapes of the e-beam were measured using YAG screens and matched well to the simulated shapes in two locations: one upstream of the alpha-magnet and one upstream of the sub-THz radiator (see Fig. 1). However, in spite of this alignment, the beam loss in the sub-THz radiator with a small vertical gap between the gratings exceeded 50% primarily due to a large electron beam emittance.

III. RADIATOR ASSEMBLY

The sub-THz radiator assembly and the gratings are illustrated in Fig. 3(a). The magnified image of the grating fragment is shown in Fig. 3(b). The side-open pair of the oversized planar copper gratings combined with a horn antenna is followed by a 2.5 cm long, ~90° permanent bending magnet. The 2.54×2.54 cm^2 magnet poles gradually open to avoid interception of the near field sub-mm wave. The electron beam exits through a thin metal foil to the left and is dumped into the external Faraday cup. The sub-THz radiation proceeds forward and exits to the air through a 3.7 cm diameter sapphire window with negligible losses. Unlike previous experiments [10], in this setup, there is no need to separate the sub-THz radiation from the electron beam by using a special mirror with a hole. A remotely controlled mechanical system is employed for fine adjustment of the vertical position of the entire assembly and the pitch angle of the structure.

The sub-THz radiator is designed to operate at a nearly $\pi/2$ phase advance (per period) of the synchronous TM symmetric eigenmode at ~0.5 THz frequency (i.e., the wavelength $\lambda = 0.6$ mm). Table II contains all essential structure parameters and dimensions. The contour plot of

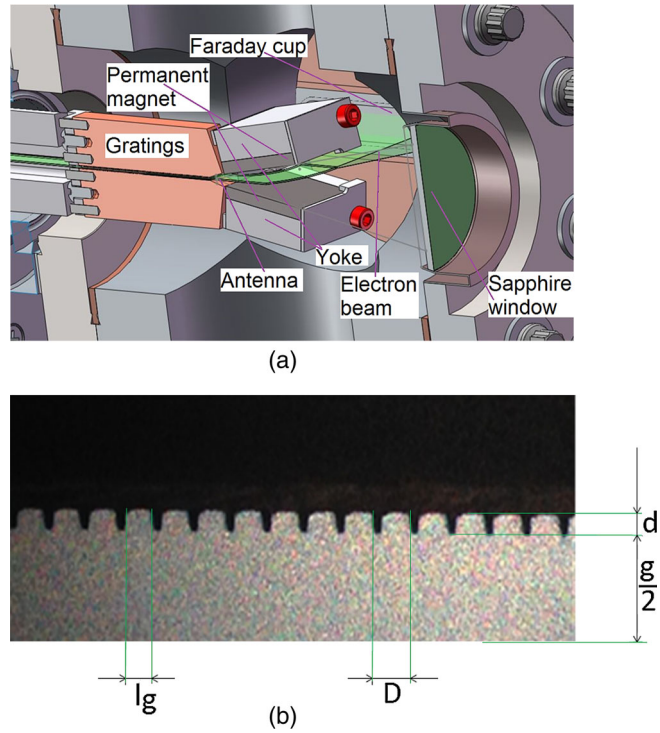

FIG. 3. Rendering of the radiator assembly (a), and a magnified photo of a 2 mm long fragment of the grating structure (b).

the longitudinal electric field across the gap is shown in Fig. 4 for the monopole-like operating mode.

The mode is well confined in both directions, but significantly extended in the horizontal direction, matching the electron beam cross section shown in Fig. 2(b). An unusual feature of the overmoded design having a width of 17λ and gap of 1.33λ is that only one well-confined, twofold symmetric fundamental eigenmode has a substantial Q-factor and effectively interacts with a flat, relativistic electron beam propagating along the axis of the structure. Other symmetric eigenmodes synchronous with the beam are either too lossy (with Q-factor significantly reduced because of the radiation through the side openings) and/or have too low coupling to the electron beam [12] (i.e., R/Q is lower by a factor of 3 or more depending on the

TABLE II. Electrodynamic and geometric parameters of the periodic slow-wave structure design.

Operating mode frequency	f	500 GHz
Q-factor	Q	~1000
Averaged shunt impedance over Q	r/Q	1.2 kΩ/m
Normalized group velocity	β_{gr}	0.8
Interaction gap	g	0.8 mm
Structure width	w	10 mm
Interaction length	L	44.5 mm
Period	D	127 μm
Groove depth	d	51 μm
Groove width	l_g	76 μm

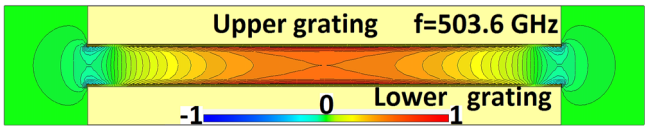

FIG. 4. Contour plot of the longitudinal electric field E_z in the transverse plane of the structure for the operating eigenmode simulated for $0.986c$ phase velocity, $f = 504$ GHz resonant frequency, and 78° phase advance.

transverse coordinates). Note, influence of the wakefield dipole and quadrupole components on the source performance is nearly negligible due to short interaction length.

Unlike mm-wave and sub-mm-wave tubes [13] and the dielectric-loaded slow-wave structure used in Ref. [10], the grating structure used in this experiment has exceptionally high group velocity, $v_{gr}\sim 0.82c$, where c is the speed of light. This has several consequences: significant shortening of the wakefield length, reduction of the wake attenuation rate, broadening of the spectrum, and enhancement of the radiated field (at a given shunt impedance [14,15]). All these effects are related to a fast movement, comparable to the particle velocity of the trailing edge of the wakefield front propagating along the dispersive slow wave structure as described in [14,16]. There are two additional benefits of the high group velocity. One benefit comes from substantially relaxed tolerances to fabrication errors and surface roughness for the gratings [12]. Another one is dispersion-enhanced sensitivity of the resonant Cherenkov frequency relative to the particle velocity. This sensitivity allowed extension of the electronic frequency tuning to relativistic beams so far only employed in conventional nonrelativistic traveling wave tubes, BWOs, and EIKs.

IV. MEASUREMENT RESULTS AND DISCUSSION

The intensity of the sub-THz radiation was measured with SDX-1223 and SPH-40 pyrodetectors from GenTEC and Spectrum Detector, respectively. Figure 5(a) shows an oscilloscope trace of the radiation registered with the pyrodetector. Figure 5(b) shows the signal dependence on the electron beam current measured with the Pearson coil. The microbunching and coherency effects are clearly manifested by the presence of the substantial quadratic component of the dependence. The sharp saturation followed by the signal reduction at higher currents as well as the presence of a linear component is due to reduction of effective interaction length caused by growing beam losses along the structure and space charge effects, resulting in bunch lengthening.

A general condition for the optimum compression of the electron bunches is maximum fast Fourier transform (FFT) of the microbunch current at the given radiation frequency [see Eq. (1)]. In our ELEGANT model it corresponds to minimum rms bunch duration σ_t near the center of the radiator structure. In experiment we obtained the optimum

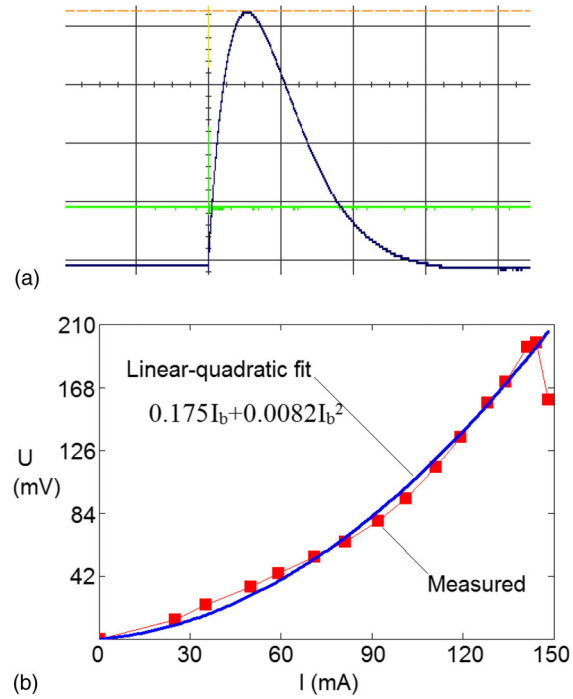

FIG. 5. Oscilloscope trace of the signal produced by the pyrodetector (a) with 100 mV and 100 μs scales per division (for the ordinate and abscise axes respectively) and the pyrodetector signal magnitude plotted as a function of the Pearson coil current (b).

by changing the alpha-magnet gradient to maximize the pyrodetector signal. It was found to be at (2.57 ± 0.12) T/m, which is in a good agreement with the value of 2.49 T/m simulated with ELEGANT without the space charge effect. Note that for a circular beam of a comparable energy, charge, and rf injector frequency, the increase of the optimum alpha-magnet gradient caused by the space charge effect appears to be more significant (~20% for 20 pC charge and 80% for 100 pC charge [17]).

Figure 6 shows spectra of the Cherenkov radiation measured by the Michelson-type interferometer [18]. Note that the spectra are averaged over several hundred of macropulses, each containing about a thousand microbunches. The FWHM of the peak, centered at the design frequency of ~0.5 THz, varied between 7.3% and 13%, depending on the electron beam energy and the gradient of the alpha-magnet. The 7.3% minimum measured bandwidth is close to the theoretical value of ~6% determined by the drain time $T_d = L(v_{gr}{}^{-1}\text{-}v^{-1})$, i.e., the difference between the filling time and the time of flight. The inhomogeneous spectrum broadening is related to pulse-to-pulse and intramacropulse variations of the peak current and the electron energy. The homogeneous broadening can be related to higher attenuation, larger gap, and reduced effective interaction length caused by the beam misalignment and the beam losses inside the structure. The interferometric results in Fig. 6 also indicate that at higher

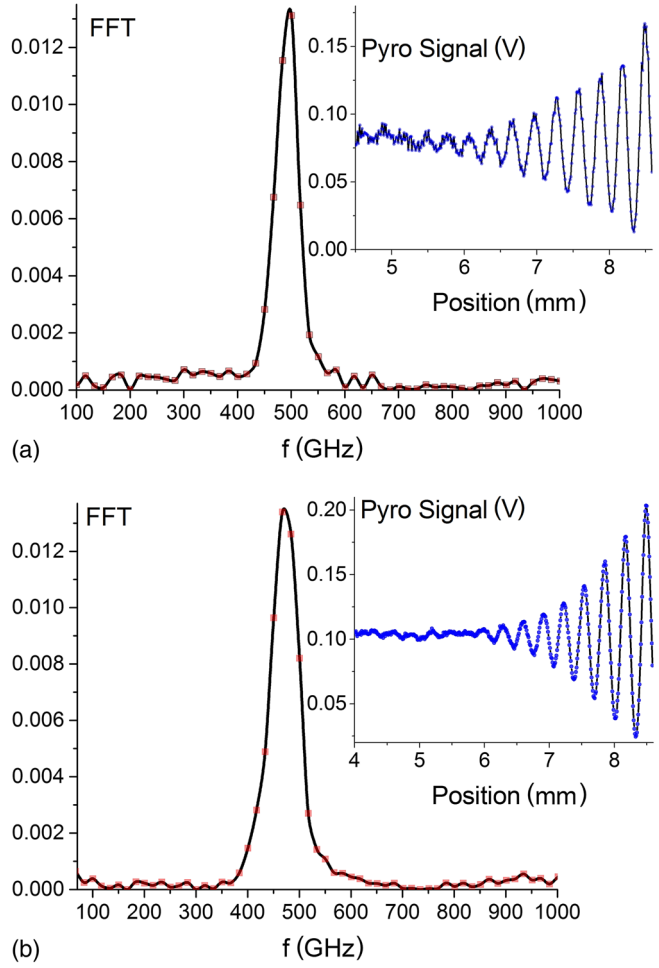

FIG. 6. Spectra of the Cherenkov radiation measured with 2.76 T/m and 2.5 MeV (a), and with 2.71 T/m and 2.9 MeV (b) alpha-magnet gradient and beam kinetic energy respectively. A half of the Fourier transform of the raw experimental interferogram is shown in the insets.

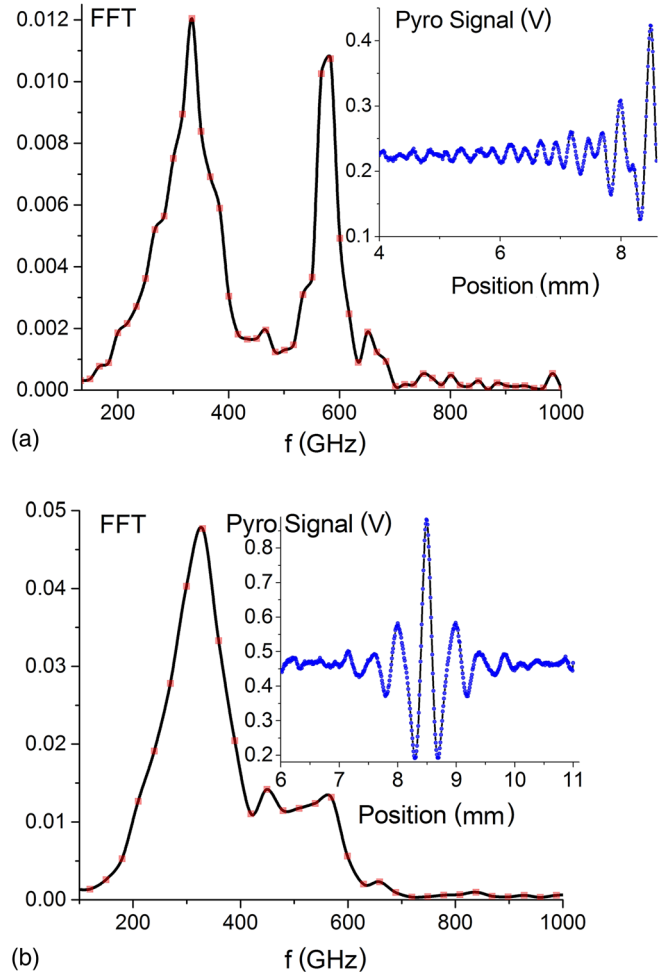

FIG. 7. Spectra of the Cherenkov radiation measured at 2.5 MeV beam kinetic energy and with 2.15 T/m (a) and 2.4 T/m (b) alpha-magnet gradients. The Fourier transform of the raw experimental interferogram is shown in the insets [one half only for (a)].

electron beam energy, the resonance frequency is lower. This is expected from the dispersion of the resonant mode of the slow wave structure at that high group velocity, which determines the enhanced frequency sensitivity to the beam voltage. In the previous experiment [10], in which the energy also changed by ~1 MeV, the electronic tuning did not take noticeable effect, because the beam was strongly relativistic (around 10.5 MeV energy), whereas the group velocity was lower ($\beta_{gr} \approx 0.3$).

The experimental interferograms shown in Fig. 7 indicate that a lower frequency signal of ~300 GHz with a much broader bandwidth of 38% can be radiated as well. This signal appears under a certain condition controlled by alpha-magnet current and the electron beam steering or mechanical alignment of the radiator.

Dozens of collected interferograms indicate that the two spectral components are tunable smoothly and reproducible within (476–584) GHz (i.e., 20%) and (311–334) GHz ranges (i.e., 7%). The frequency was tuned mostly with beam energy, whereas the intensity of each of these frequency components was controlled relatively independently from zero to maximum by fine-tuning of the beam transport within the structure.

The appearance of the two frequency components of the Cherenkov radiation from a relativistic beam presents a new phenomenon resulting from the features of wakefield excitation in the side-open overmoded structure that may also support lower frequency synchronous modes (including dipole-like asymmetric modes). A similar effect is observed in simulations with longer bunches in [12]. As illustrated in Fig. 8, the generation of lower than the fundamental frequency (~300 GHz versus ~500 GHz) occurs at longer bunch lengths (>200 μm) and when the beam is displaced horizontally by a few mm from the axis of symmetry. This correlates with the experimental observation of the lower frequency in Fig. 7. For example, for

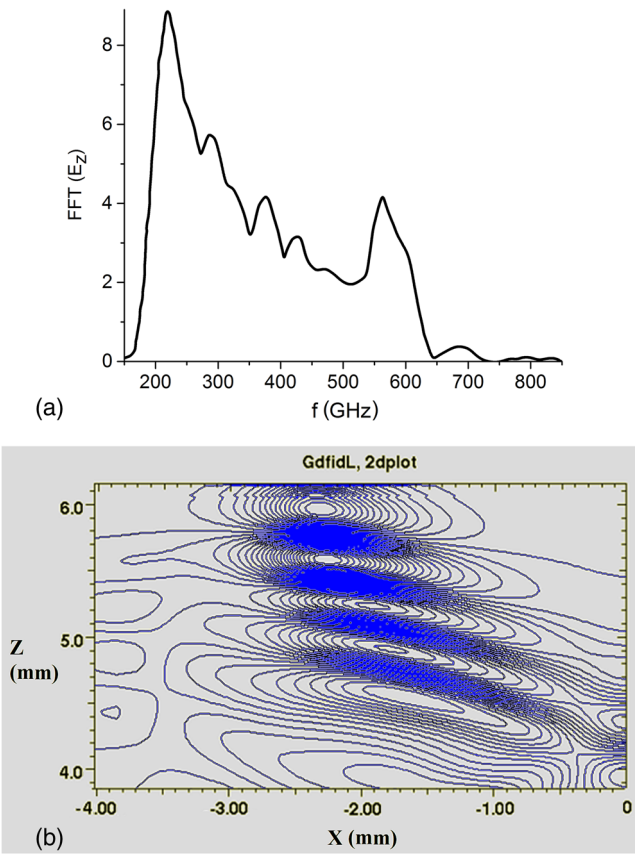

FIG. 8. GDFIDL simulation of asymmetric wakefield for the model of gratings structure with 40 periods and 5 mm width designed to operate at ~500 GHz frequency: (a) FFT for longitudinal field E_z at $z = L$ and (b) E_z contour plot in the median plane at $t = 24$ ps. Filament microbunch with Gaussian distribution has $\delta_z = 250\ \mu$m rms length and $x = -2.5$ mm horizontal offset. The structure axis of symmetry is located at $x = 0$.

Fig. 7(a), the alpha-magnet gradient is only 2.15 T/m vs the (2.71–2.76) T/m gradient for Fig. 6 at the same beam energy (see captions in Figs. 6 and 7), and also vs the ~2.5 T/m optimal gradient found in simulations. This means that the bunch length for Fig. 7 is certainly longer than the one in Fig. 6.

Energy density radiated into the sub-mm waves was measured first with the SPH-40 pyrodetector employing a $LiTaO_3$ 50 μm thick, 2.5×2.5 mm^2 element with chromium coating. The detector was placed at about a distance of 2.5 cm from the sapphire window and displaced by about 1 cm vertically with respect to the axis of the radiating structure symmetry. This displacement takes into account specifics of the far field radiation pattern having two vertically wide and horizontally narrow radiation lobes with zero on-axis intensity [15]. The maximum energy density of the radiation impinging on the sensitive area of the detector was found to be $\geq 50\ \mu$J/cm^2 per macropulse. In the interferometer setup (i.e., with three mirrors downstream the sapphire window, see Fig. 1) the energy density of 12 μJ/cm^2 was measured with the SDX-1223 THZ5I-BL-BNC detector factory-set as a joulemeter. The detector employs a 50 μm thick, 5×5 mm^2 $LiTaO_3$ crystal with a 400 μm black carbon organic coating on the top of the 50 μm chromium coating.

One can calculate analytically the energy radiated by a single microbunch for our well-matched horn antenna, neglecting the return losses according to the electromagnetic design [15]. For a closed rectangular corrugated configuration, the energy radiated can be obtained with the direct wakefield calculations [19]. In more general configurations, the radiated energy can be calculated with the eigenmode excitation theory applied in time domain [14] as follows:

$$W_{1b} = \frac{\omega}{4}\frac{r}{Q}\frac{L}{|1-\beta_{gr}/\beta|}\left(q\Phi\frac{1-\exp(-\alpha L)}{\alpha L}\right)^2, \qquad (1)$$

where q is the bunch charge, $r = {E_z}^2/(dP/dz)$ is the shunt impedance, $\omega = 2\pi f = h(\omega)/v$ is the resonance circular frequency, $h = 2\pi/\beta\lambda$ is the wave number within the structure, $\beta = v/c$, $k = \omega/c$, Q is the Q-factor, $Q|\beta\text{-}\beta_{gr}| \gg 1$, $\alpha = \pi f/Qv_{gr}$ is the attenuation, $\Phi = \frac{1}{q}\int \eta(z')\exp(-ik\frac{z'}{\beta})dz'$ is the bunch form factor, and η is the bunch linear density. For a Gaussian bunch with the rms duration $\sigma_t = \delta_z/v$ the form factor can be calculated as $\Phi = \exp[-(\omega\sigma_t)^2/2]$.

From a comparison of the spectra of Fig. 6 with GDFIDL simulations, we estimate the microbunch length $\delta_z <$ 150 μm. From Eq. (1), Table I, and Table II we obtain (25–170) nJ energy radiated per microbunch at ~500 GHz resulting in (0.7–5) kW peak power (the minimum energy corresponds to the maximum bunch rms length 150 μm). This corresponds to (18–121) μJ per rf macropulse and (72–480) W macropulse power giving up to 1.8 mW average power at 15 Hz pulse repetition rate. The maximum macropulse energy density estimated from the pyrodetector measurements is within the analytical estimation.

Thus, the measurements indicate that energy per rf macropulse and the average power of sub-THz radiation exceed that obtained in [10] with 10–11 MeV electron beam.

V. SUMMARY

A sub-THz, narrow bandwidth coherent Cherenkov radiation was produced on a tabletop beam line. A 2–3 MeV electron beam is generated by an S-band thermionic cathode rf electron gun, compressed by a compact alpha-magnet, and finally sent through a novel radiator that employs a planar, side-open, noncapillary, dielectric-free, copper structure capable of withstanding significant beam losses. The flat beam configuration in the radiator allows the transport of a substantial charge. With the addition of collimation and cooling, such a structure may operate at

high repetition rates producing high average power of sub-THz radiation [20].

The radiator design allows changing the radiation spectrum using beam steering and by varying the beam energy. To the best of our knowledge, such tuning has not yet been demonstrated with a relativistic electron beam in coherent Cherenkov radiation systems. That feature can be used for a number of applications, in which frequency adjustability is required (e.g., in spectroscopy for identification of specific trace molecules). The overmoded structure with high group velocity and aperture gap exceeding the radiation wavelength supports efficient radiation at a single fundamental mode.

The experiment described above demonstrates good potential for a compact, robust, laser and undulator-free, tabletop system for the generation of a narrow bandwidth sub-THz radiation. This setup can be considered as a prototype of a highly efficient sub-mm-wave source capable of operating in a long-pulse multibunch (or even continuous) mode driven by a rf injector.

A similar structure can be efficiently utilized for other applications, e.g., for time-dependent beam diagnostics or to remove unwanted time-dependent energy variations in longitudinally compressed electron bunches using longer wavelengths [21–25].

ACKNOWLEDGMENTS

This work was supported by the U.S. Department of Energy (Award No. DE-SC-FOA-0007702). The authors acknowledge Warner Bruns for the GDFIDL code license, Bas van der Geer and Marieke de Loos for the General Particle Tracer (GPT) code simulations, Don Dooley and Sid Levingston for the data on pyrodetector calibration and performance in the sub-THz region, Albert Hillman, Shifu Xu and Steven Shoaf for their help with magnet power supplies and controls, and Emma Curry for recalibration of the pyrodetectors at UCLA.

[1] Opportunities in Terahertz (THz) Science–Office of Science DOE report, http://science.energy.gov/~/media/bes/pdf/reports/files/thz_rpt.pdf.

[2] N. A. Vinokurov, Status, and perspectives of the FEL at Novosibirsk Center of Photo-Chemistry Research, www.kinetics.nsc.ru/center/public/st05.pdf; S. V. Miginsky, N. A. Vinokurov *et al.*, in *Proceedings of the 4th Asian Particle Accelerator Conference, Indore, 2007* (RRCAT, Indore, India, 2007), p. 616.

[3] G. L. Carr, M. C. Martin, W. R. McKinney, K. Jordan, G. R. Neil, and G. P. Williams, Nature (London) **420**, 153 (2002).

[4] S. Chattopadhyay, S. T. Corneliussen, and G. P. Williams, in *Proceedings of the 9th European Particle Accelerator Conference, Lucerne, 2004* (EPS-AG, Lucerne, 2004), p. 2454.

[5] W. P. Leemans *et al.*, *Phys. Rev. Lett.* ***91****, 074802 (2003)*.

[6] DOE-NSF-NIH Workshop on Opportunities in THz Science, Opportunities in THz Science Report of a DOE-NSF-NIH Workshop, 2004, Arlington, VA, edited by M. S. Sherwin, C. A. Schmuttenmaer, and P. H. Bucksbaum, http://www.sc.doe.gov/bes/reports/files/THz_rpt.pdf.

[7] J. M. Byrd, Z. Hao, M. C. Martin, D. S. Robin, F. Sannibale, R. W. Schoenlein, A. A. Zholents, and M. S. Zolotorev, Phys. Rev. Lett. **96**, 164801 (2006).

[8] K. Holldack, S. Khan, R. Mitzner, and T. Quast, Phys. Rev. Lett. **96**, 054801 (2006).

[9] G. P. Gallerano and S. Biedron, in *Proceedings of FEL2004 Conference* (Comitato Conferenze Elettra, Trieste, Italy, 2004), p. 216.

[10] A. M. Cook, R. Tikhoplav, S. Y. Tochitsky, G. Travish, O. B. Williams, and J. B. Rosenzweig, Phys. Rev. Lett. **103**, 095003 (2009).

[11] M. Borland, *User's Manual for elegant* (Advanced Photon Source, Lemont, IL, 2011).

[12] A. V. Smirnov *et al.*, in *Proceedings of the 25th Particle Accelerator Conference, PAC-2013, Pasadena, CA, 2013* (IEEE, New York, 2013), p. 925.

[13] J. X. Qiu, B. Levush, J. Pasour, A. Katz, C. M. Armstrong, D. R. Whaley, J. Tucek, K. Kreischer, and D. Gallagher, IEEE Microw. Mag. **10**, 38 (2009).

[14] A. V. Smirnov, Nucl. Instrum. Methods Phys. Res., Sect. A **480**, 387 (2002).

[15] A. V. Smirnov, Nucl. Instrum. Methods Phys. Res., Sect. A **771**, 147 (2015).

[16] E. L. Burshtein and G. V. Voskresenskii, Linear Accelerators of Electrons with Intense Beams (Atomizdat, Moscow, USSR, 1970), in Russian.

[17] H. Hama *et al.*, in *Proceedings of the 2008 Free Electron Laser Conference, Gyeongju, Korea* (American Physical Society, 2008), p. 305, http://accelconf.web.cern.ch/AccelConf/FEL2008/papers/tupph029.pdf.

[18] http://www.radiabeam.com/products/Interferometers.html.

[19] K. L. F. Bane and G. Stupakov, Phys. Rev. ST Accel. Beams **6**, 024401 (2003).

[20] R. Agustsson, S. Boucher, T. Grandsaert, J. J. Hartzell, M. Ruelas, A. V. Smirnov, S. Storms, Y. Kim, A. Andrews, B. Berls, C. F. Eckman, K. Folkman, A. Hunt, A. E. Knowles-Swingle, C. O'Neill, M. Smith, and P. Buaphad, in *Proceedings of the 4th International Particle Accelerator Conference, IPAC-2013, Shanghai, China, 2013* (JACoW, Shanghai, China, 2013), p. 2295.

[21] K. Bane *et al.*, Corrugated pipe as a beam dechirper, Report No. SLAC PUB-14925, 2012.

[22] M. Harrison *et al.*, in *Proceedings of the Free Electron Conference, Basel, Switzerland* (JACoW, 2014), p. 788, http://accelconf.web.cern.ch/AccelConf/FEL2014/papers/thp034.pdf.

[23] P. Emma *et al.*, Phys. Rev. Lett. **112**, 034801 (2014).

[24] S. Antipov, S. Baturin, C. Jing, M. Fedurin, A. Kanareykin, C. Swinson, P. Schoessow, W. Gai, and A. Zholents, Phys. Rev. Lett. **112**, 114801 (2014).

[25] F. Fu *et al.*, Phys. Rev. Lett. **114**, 114801 (2015).